SPACE TELESCOPE SCIENCE INSTITUTE
Operated for NASA by AURA

Instrument Science Report: STIS 2012-02

Post SM4 behavior of STIS CCD darks

E. Mason

October 5, 2012

Abstract

Following Servicing Mission 4 (SM4) and the resumption of STIS operations, the STIS CCD detector has shown an increased dark current and a significant scatter of the average dark current about the mean or median. The increase of the dark current is consistent with the trend observed before STIS failure and is due to the CCD aging. The larger scatter is explained by the significant fraction of pixels that deviate from the ideal case. The larger pixel noise, is most likely caused by the (parallel) charge transfer inefficiency (CTI).

1. Contents

- The pipeline temperature relation and reference dark
- Summary and conclusion

2. Introduction

STIS was installed on HST in 1997 and is one of the 2^{nd} generation instrument on board. It has been operational since Apr 1997. STIS has suffered two major malfunctions. The first was in May 2001, when the side-1 electronics failed, and then in 2004 when the side-2 power supply failed. The 2001 failure changed the operational mode of the instrument (see below), as STIS operations could continue using the redundant side-2 electronics. However, the 2004 failure rendered the instrument inoperable. STIS operations were recovered only in 2009 during Servicing Mission 4 (SM4), when the failed card in the side-2 electronics was replaced. Since May 2009, after almost 5 years of "black-out", STIS has been fully operational again with the repaired side-2 electronics.

Active, closed-cycle thermal control with side-2 electronics is not possible due to the lack of a working temperature sensor for the CCD detector. The STIS CCD has been run with constant current, rather than at constant temperature, since May 2001. The result is that the detector is subject to temperature variations as a consequence of the telescope and instrument thermal cycles. CCD characteristics such as dark current and bias level depend on the temperature of the detector; given that this is not constant, the STIS CCD dark current and bias level fluctuate. Each science exposure will have its own bias level and dark current which depend on the actual (unknown) temperature of the detector at the time of the observation. This must be (and is) taken into account when processing the data within CALSTIS. In particular, the dark current was found to correlate with the temperature of the CCD-housing (Brown 2001a), and, since then, a linear scaling of the dark frames has been implemented in the CALSTIS pipeline and the data reduction chain.

After SM4 the CCD characteristics and performances were newly determined and compared with those before the 2004 failure (Goudfrooij et al. 2009). Goudfrooij et al. found that most aspects of the detector performance were either consistent with past ones or with the extrapolation of the observed, "pre-2004 failure" trends. In particular the dark current of $\sim$0.012 e^-/sec is roughly consistent with the extrapolation of the dark current trend observed in the period 2001-2004, and with the yearly increase of 2.2-3.3 e^-/hr/pix/yr reported by Sirianni et al. (2002). However, after a few months of operations and monitoring it soon became apparent that the average dark current showed a large un-foreseen scatter (see Fig.1).

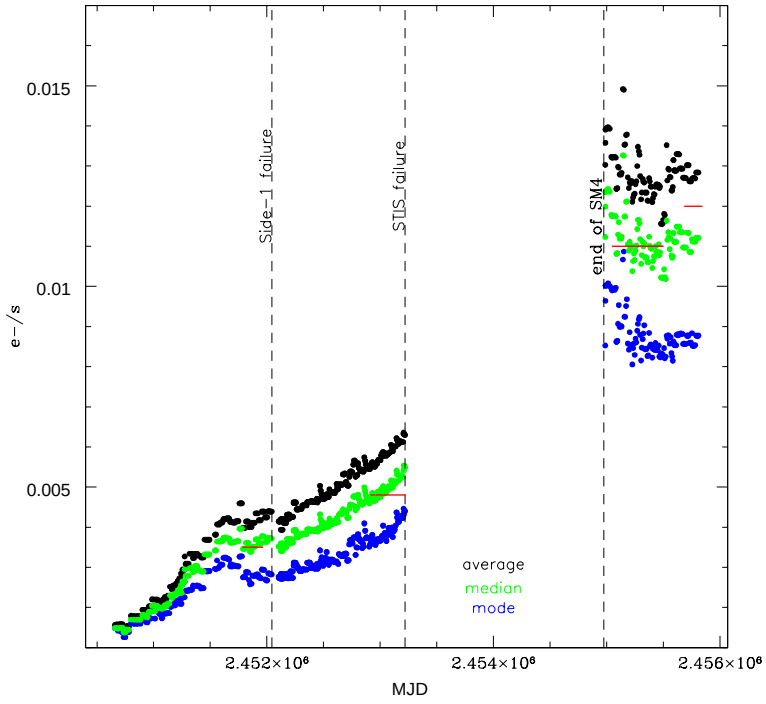

Fig. 1.— *The evolution of STIS CCD dark current versus time. The average (black), median (green), and modal (blue) dark current were measured in the reference frames produced by the pipeline. Dashed vertical lines mark the major events that occurred during the STIS lifetime. Horizontal red lines mark the periods corresponding to programs 8837 (cycle 9), 10017+10018 (cycle 12), 11844+11845 (cycle 17), and 12401 (cycle 18), analyzed in this ISR.*

3. The data-set

As part of the STIS calibration plan, dark frames are taken regularly within each cycle. In particular, ∼13-17 dark exposures, each 1100 sec long, are taken every week as part of the dark monitoring plan. In order to investigate the large scatter of the average dark current, we analyzed the 1100 s dark exposures taken within the following programs:

- 8837 (i.e. from Aug 2000 to Feb 2001, cycle 9, side-1 operations)
- 10017/18 (i.e. from Oct 2003 to Aug 2004, cycle 12, side-2 operations)
- 11844/45 (i.e. from Aug 2009 to Oct 2010, cycle 17, post SM4 side-2 operations),
- 12401 (i.e. from May 2011 to Oct 2011, cycle 18, post SM4 side-2 operations)

4. The evolution of the dark current and the pixel distribution

In this section we discuss the statistics of the pixel values in both reference and single dark frames. In all cases the statistics were computed adopting a multi-cycle σ-clipping algorithm, to remove the most deviant pixels from the analysis and obtain a good representation of the average pixel. We verified that adopting thresholds at 3σ and repeating the σ-clipping over 30 cycles, effectively removed from our analysis the hot pixels ($\sim$2% in cosmic-ray cleaned and combined frames) and cosmic rays (which have not been removed in the single frames and affect about 3-4% of the pixels). However, we also removed a fraction of warm pixels ($\sim$5-10%) as each data point results from the average of $\sim$87-89% of the total number of pixels. Hence, the computed average and standard deviation are slightly smaller than in the real case and possibly represent a lower limit.

Fig. 1 shows the average (black), the median (green), and modal (blue) dark current as measured on the reference dark frames produced by the pipeline (Diaz 2004). As mentioned already in the previous section, the figure shows that the instrument dark current has increased with time (as expected), and that the scatter of the data points is significantly larger than before the 2001 failure. However, it should also be noted that:

1. the scatter is larger when the average (or median) dark current is computed, rather than the mode. This might imply that there is a relatively large and variable number of *warm* pixels entering into the statistic;

2. the scatter is possibly slightly decreasing since SM4, especially if the mode is considered. This might imply that, following the period of no-operations and the installation of the new instrument, COS, STIS and its CCD were not in stable conditions (e.g. thermally stable).

The data points in Fig. 1 are computed from normalized average frames and, in order to understand the origin of their scatter, it is mandatory to inspect each single frame coming into play. Fig. 2 plots the average integrated dark current measured in single dark exposures taken during cycle 9, 12, 17, and 18. The frames had the bias level determined from the overscan subtracted using CALSTIS before computing the statistics. The figure plots the statistics on the upper part of the CCD only (top 374 rows, black dots), which includes the E1 position for spectroscopic observations and is less affected by charge-transfer-inefficiency (CTI). However it should be noted that computing, alternatively, the statistics on the whole detector or its bottom part, does not change the conclusion herein, except that the charge traps and the reduced charge-transfer-efficiency (CTE), increase the average values while reducing their standard deviation (STDDEV, see section 5 and Fig. 3).

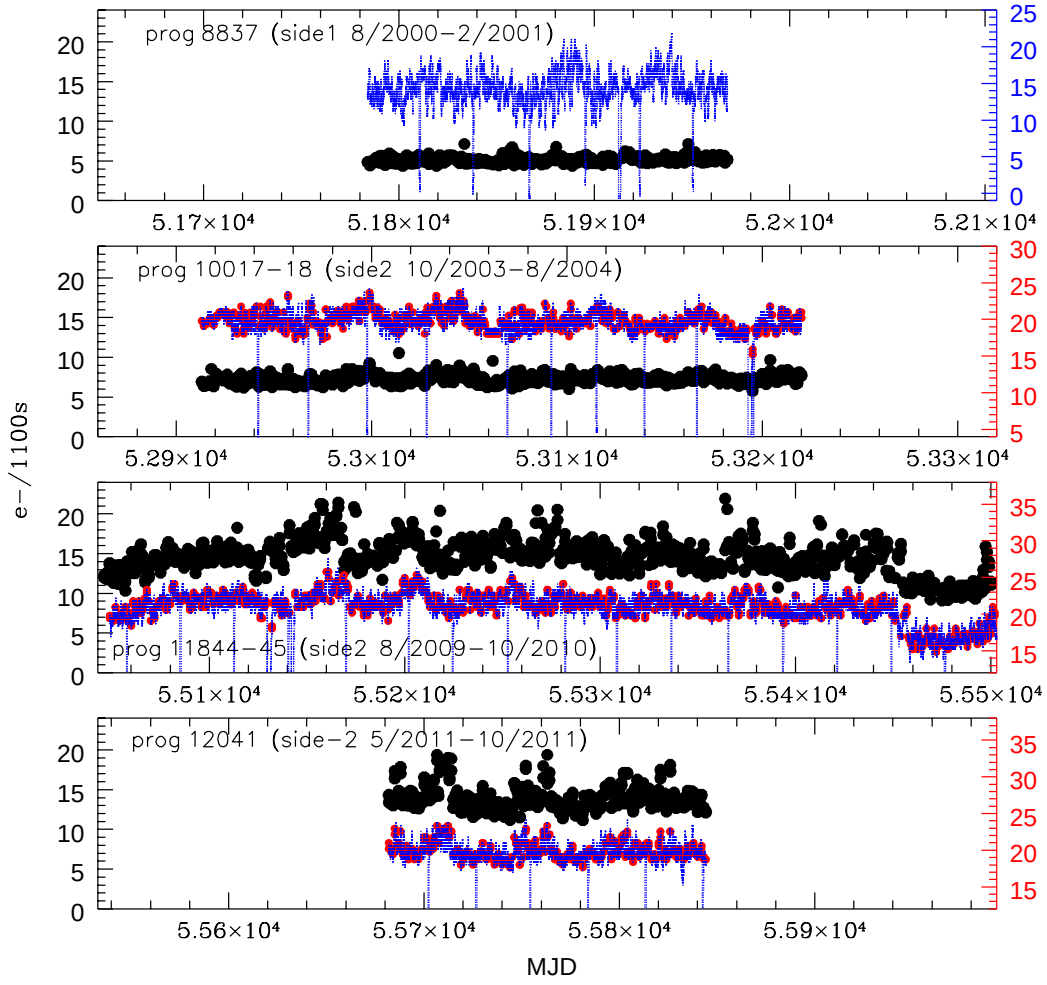

Fig. 2.— *The average dark current (black circles) measured in the dark frames taken within the dark monitoring programs 8837 (top panel), 10017 & 10018 (second panel from the top), 11844 & 11845 (third panel from the top), and 12401 (bottom panel). The individual dark frames were only overscan subtracted. Blue dots represent the telemetry records of the CCD-housing temperature, while the red circles represent the OCCDHTAV records in each image header. Note that the OCCDHTAV entry was added only after the failure of the Side-1 electronics. All three panels have same x and y ranges for an easier comparison. The y-axis on the left report the (integrated) average dark current (in e-/1100 sec), and, on the right, the temperature (in degree Celsius). See text for more details.*

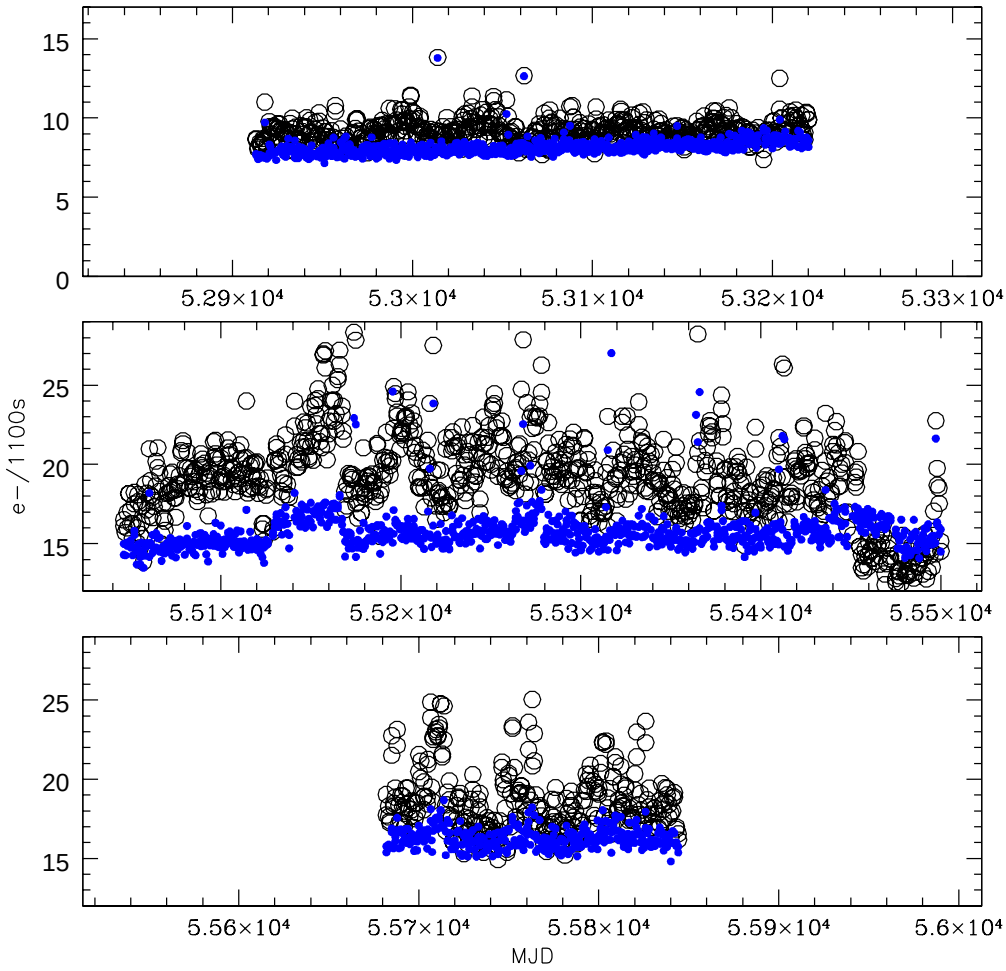

Fig. 3.— *The average dark current (black circles) measured in the dark frames taken within the dark monitoring programs 10017 & 10018 (top panel), 11844 & 11845 (mid panel), and 12401 (bottom panel). The individual dark frames were only overscan subtracted and the statistic was computed on the whole area of the CCD. Blue circles represent the average dark current of the same frames after having been scaled to the reference temperature of 18 C (see Brown 2001a). Note that at least a few of the most deviant points in the mid panel correspond to dark exposures taken in proximity of the South Atlantic Anomaly (SAA). The SAA contours for the dark monitoring program were revised during cycle 19.*

Fig. 2 also shows the telemetry records of the CCD-housing temperature (blue dots) and the CCD-housing temperature recorded in each image header[1](red circles). During side-1 operations (top panel of Fig. 2) the CCD dark current was not correlated with the CCD-housing temperature, as, in fact, the detector temperature was actively controlled and maintained at a constant value, while the CCD-housing temperature correlated with the heat input to STIS. Once the operations were moved to side-2, the dark current and the CCD-housing temperature started to be correlated.

Fig. 3 shows the effectiveness of the temperature scaling relation in use. Black circles represent the average integrated dark current measured in the single dark exposures taken during cycle 12, 17 and 18 and computed on the whole CCD area. Blue circles represent the average integrated dark current measured in the same frames after having scaled them for the temperature relation determined by Brown (2001a). Though it significantly reduces the scatter of the data points, part of that scatter appears independent of the temperature.

In summary, Fig. 2 & 3 show that, after SM4, the CCD dark current

1. has increased in value as expected because of radiation damage,
2. remains correlated with the CCD-housing temperature,
3. the in-use temperature scaling relation remains valid
4. has a larger scatter after SM4 than it had during 2001-2004 side-2 operations. This is intrinsic to the detector and temperature independent. It is not a pipeline artifact introduced when the reference darks are created.

The presence of the detector in a harsh space and radiation environment contribute to the degradation of the silicon structure, increasing the dark current and the number of warm and hot pixels. This is shown in Fig. 4, which plots the pixel distribution of **a** few dark frames taken at different epochs. The pixel distribution (Fig. 4) has broadened with time developing a large tail of warm and hot pixels. While the hot pixels are flagged and might be ignored in the data reduction process, the warm pixels affect the statistics calculated on the frame. The skewed distribution implies that mode and mean are significantly different, with the mean no longer accurately representing the bulk of the pixel distribution. We should note, however, that the mode cannot readily replace the mean, as the former is not a robust statistical parameter, nor does it allow for computation of rigorous error propagation.

[1]The value was effectively recorded only after the 2001 side-1 failure.

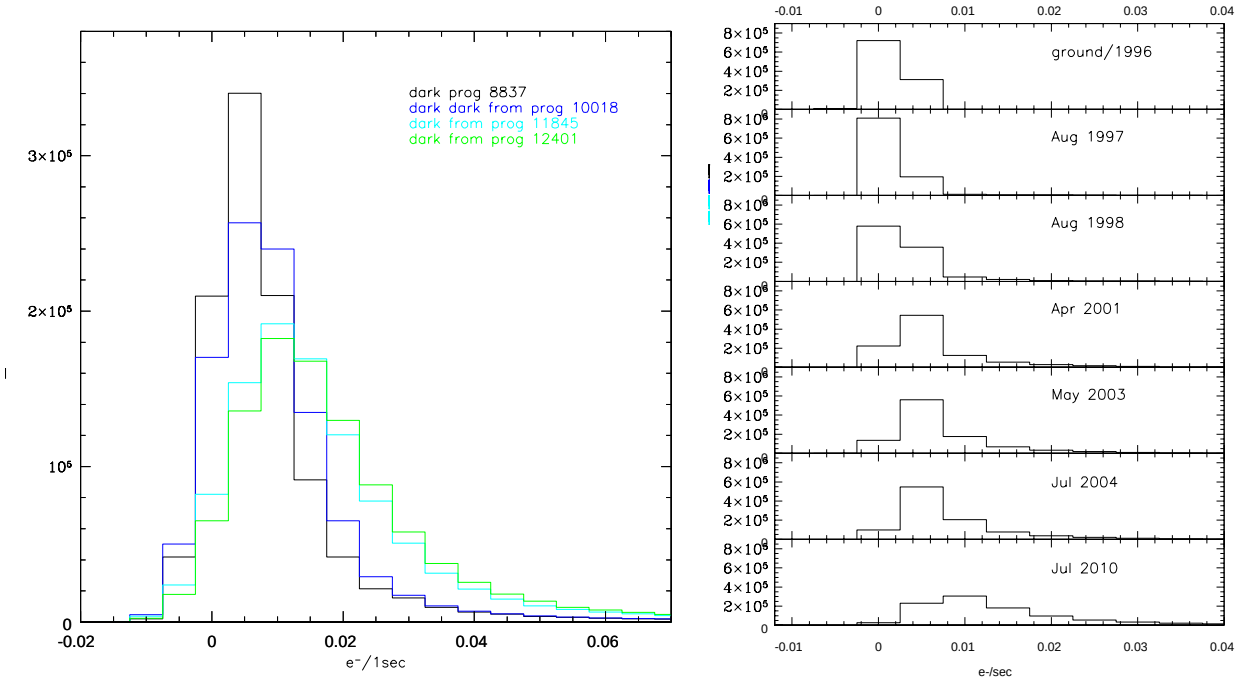

Fig. 4.— *Left panel: the pixel distribution of 4 darks frames taken from the darks monitoring program 8837, 10018, 11845 and 12401. They have all the same CCD-housing temperature, T=18.036 C and have been normalized to 1 sec of exposure time for an easier comparison with the reference dark distribution (right panel). Color coding is on the figure itself. Right panel: pixel distribution of 7 reference darks taken across STIS life. Each dark has been plotted on a separate sub-panel for clarity. The epoch of each reference dark is marked in each sub-panel. Y and X axis range are the same in each sub-panel for an easier comparison.*

5. The STDDEV of the individual pixel

Larger dark currents imply larger Poisson noise and, therefore, a larger scatter of the data points. Hence, in order to establish whether the observed dark current scatter is consistent with the increased dark current value, we evaluated the standard deviation of individual pixels and compared that with "well behaving Poissonian pixels". In particular, we computed the statistics for each single pixel in a relatively large sample (125) of darks taken all at the same temperature (T=20.977 C) during cycle 17. The frames were corrected only for overscan and were not combined to remove the cosmic rays. In order to exclude the cosmic ray hits from the statistic we focused only on those pixels which had at least 90% of good records (i.e. 112 over 125 records). We then computed the pixel statistic of the

good records only, discarding the bad ones. We considered a "good record" any pixel value which was below the hot pixel threshold used within the CALSTIS pipeline. This corresponds to $0.1\,e^-$/sec/pix in a normalized dark scaled at the reference temperature of T=18.0 C or, equivalently, to $132\,e^-$/pix in a 1100 sec dark frame taken at the CCD-housing temperature T=20.977 C.

We computed the statistics of each single pixel and compared with that of an ideal pixel having the same average value and noise corresponding to $\sqrt{RON^2 + (\text{DARK SIGNAL})}$. This is shown in Fig. 5 (left panel) were we plot each "good" pixel STDDEV versus its average value. The black dots represent the pixels across the whole frames, while green and light-blue dots represent pixels from the top and bottom part of the CCD, respectively. We also plot the ideal "photon transfer curve"(bottom solid red line), as well as a number of simulated measurements (cyan crosses) for a set of ideal pixels with different average dark current (e.g. 11, 21, $31\,e^-$/1100 sec). The number of simulated measurements per pixel value is equal to the actual number of pixels observed at that given value. This was done in order to show the scatter of the data point we should expect if the pixels were all "well behaved". The top red line is the upper limit 3σ above the ideal curve.

The figure is showing that a significant fraction of the pixels deviates from the ideal case and has a STDDEV which is significantly above the expected value. In addition, analyzing separately the top and bottom part of the CCD we find that they behave similarly and deviate in a similar way from the ideal case, though, as mentioned before, the average dark current in the pixels in the bottom part of the CCD tend to be higher.

Note that the "photon transfer curve" does not change if darks taken within a same annealing period and scaled to a common reference temperature are analyzed in place of the sample above. Hence, the large STDDEV are not due the change of the pixels dark current between one annealing period and the next (or, at least, not in a statistical sense).

The right panel of Fig. 5 shows the distribution of the observed (black line) and expected (cyan line) STDDEV for the pixels with average dark current $\sim 15\,e^-$. The observed distribution is significantly skewed and the majority of the pixels has a STDDEV which is significantly larger than the expected Poisson+readout noise. As much as each pixel has a larger noise than the theoretical one, the resulting average dark current (per frame) will also have a larger STDDEV. In addition, the pixel-to-pixel dark current correction will be overestimated in some pixels and under-estimated in other, producing a salt-and-pepper noise in the corrected frames.

We conclude this section noting that the "additional" pixel noise which we observe, does not appear to be correlated with the telescope and/or instrument setup. We tested the 125

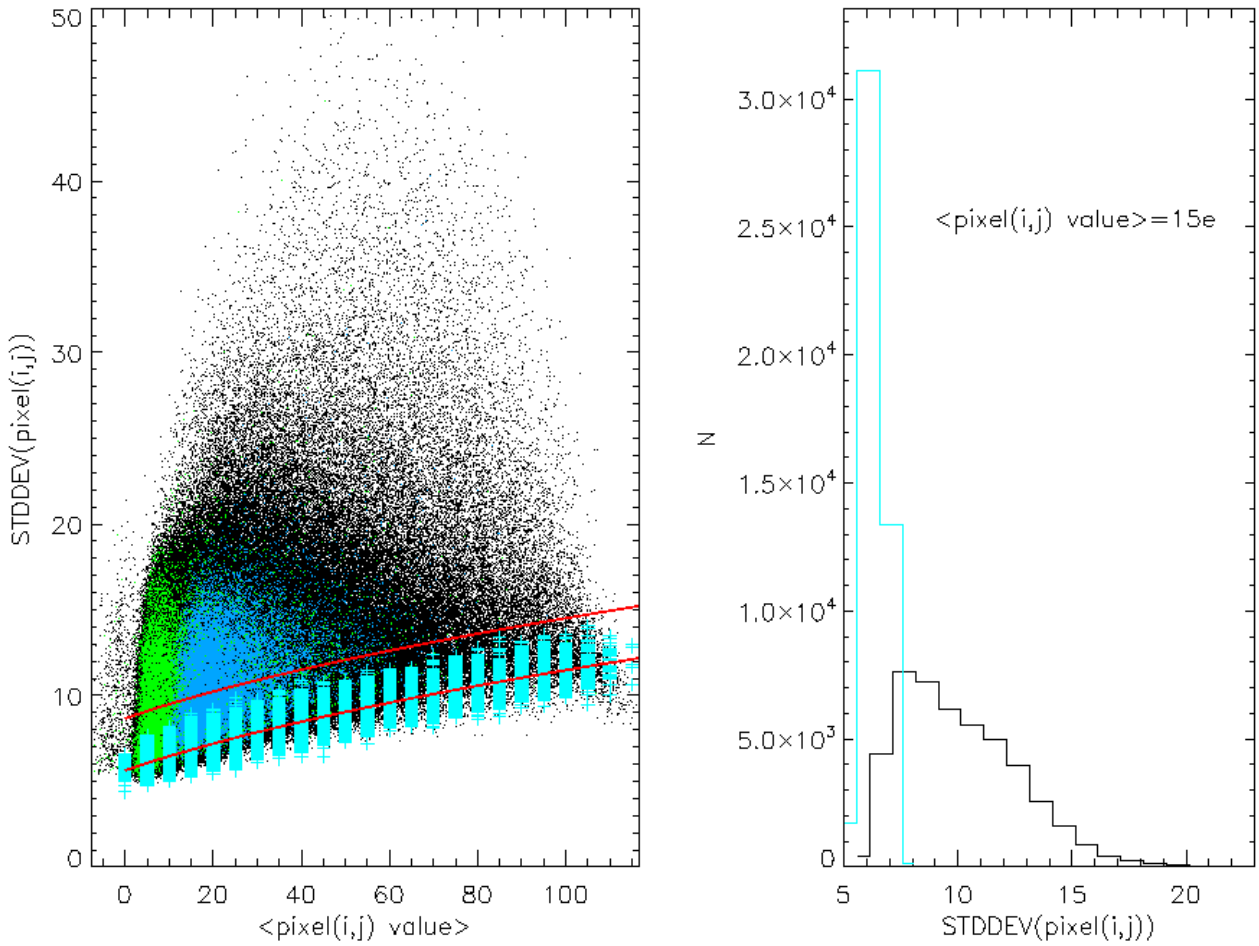

Fig. 5.— *Left panel: The STIS CCD photon transfer curve (though not in log scale). Black dots represent the pixels from the whole detector; while green and light-blue dots represent pixels from the top and the bottom part of the detector, respectively. Each dot represents a pixel which had at least 112 good values over a total of 125 images. The solid red lines represent the ideal photon transfer curve (bottom one) and the average 3σ upper limit (top one). The cyan crosses represent, each, an ideal pixel. Together with the red lines they should give an idea of the spread of the points, which we should observe if the CCD was following the ideal case. Right panel: distribution of the pixels* STDDEV *for pixel values in the range 14.5-15.5* e^-*. The black histogram represents the observed distribution, while the cyan color represents the ideal case.*

dark frames against several setup keywords recorded in each image header[2], and the bright earth pointing, finding no correlation.

6. The pixel statistic across the frames

STIS CCD has three overscan regions: two of size 19 columns by 1044 rows on the left and right side of the detector and one of size 1024 columns × 20 rows on the bottom part of the detector (see Fig 6). The left and right overscan are physical: they correspond to 19×1 physical and unexposed pixels at the end of each serial register[3], which are read out together with each row once it has been clocked/transferred in the serial register. The bottom overscan is virtual and generated by additional detector clocking *after* all of the exposed rows of the CCD have been read out. The parallel and serial clocking of the STIS CCD are along the columns, from bottom to top, and along the rows, from left to right, respectively, for the currently in use amplifier (Fig. 6). For this reason the left and right overscan are alternatively called "serial overscan". The bottom overscan is more commonly addressed as the "virtual overscan". Note that, being clocked after the readout of the exposed CCD, the virtual overscan collects released charges from charge traps and displays trails similarly to the exposed CCD.

The overscan regions, similarly to the bias frames, provide information on the zero offset (the bias level) of the frame and its uncertainty. Ideally serial and virtual overscan and bias frame should deliver similar and consistent information, though the bias frame has the advantage of mapping 2D patterns of the zero level. Therefore, in order to constrain the nature of the pixel noise and possibly establish whether the observed behavior should be ascribed entirely to parallel CTI or not, we compared:

- the bias/zero level of the 3 overscan regions
- the standard deviation of the 3 overscan regions
- the behavior of the overscan region with respect to the exposed part of the detector.

In doing this, we considered raw dark frames, which have not been corrected for bias and/or

[2]The actual parameters inspected were: RA_APER, DEC_APER, PA_APER, ORIENTAT, SUNANGLE, SUN_ALT, MOONANGL, OSWABSP, OMSCYL1P, OMSCYL3P, OMSCYL4P, OCBABAV, OCBCDAV, OCBSWALV, OCBRCDLV, OCCDHTAV, PRIMESI.

[3]STIS CCD has 2 serial registers: on the bottom and the top sides of the detector.

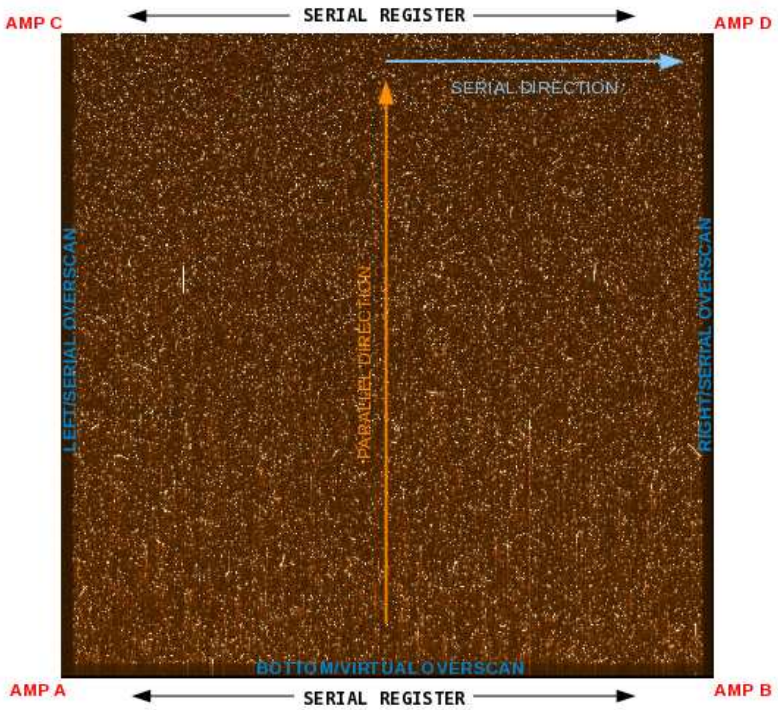

Fig. 6.— *A typical STIS CCD dark exposure with the detector layout marked. Note that, while the CCD can be read out through any of the 4 amplifiers (also marked in the figure); the one currently in use is amplifier D.*

overscan. We selected frames taken either at temperature T=19.447 C or T=20.977 C, during cycle 12 and 18.

The bias level as measured from the three overscan regions (left-serial, right-serial and bottom-virtual overscan) do not have matching average values but the following relation holds: $\overline{\text{RIGHT SERIAL OVERSCAN}} < \overline{\text{LEFT SERIAL OVERSCAN}} < \overline{\text{VIRTUAL OVERSCAN}}$ (Fig. 7). In particular, the right and left serial overscan differ, typically, by 3-4 e^-, while the virtual and the left serial overscan differ by $\sim$ 8-10 e^-. The serial overscan which is closer to the readout amplifier (i.e. the right serial overscan for the readout through amplifier D) presents a sudden drop of the zero level (roll-off) in the $\sim$4 pixels which are immediately adjacent to the amplifier. For this reason Goudfrooij and Walsh (1997) have identified optimal overscan "sub-region" over which is safe to estimate the bias/zero level. However, we observe that, even using Goudfrooij and Walsh safe overscan region, the serial overscan which is closer to the readout amplifier (whether D, C or A) tends to have slightly lower average zero level. This is true for frames taken during any cycle, and in particular, also for cycle 8 data, which

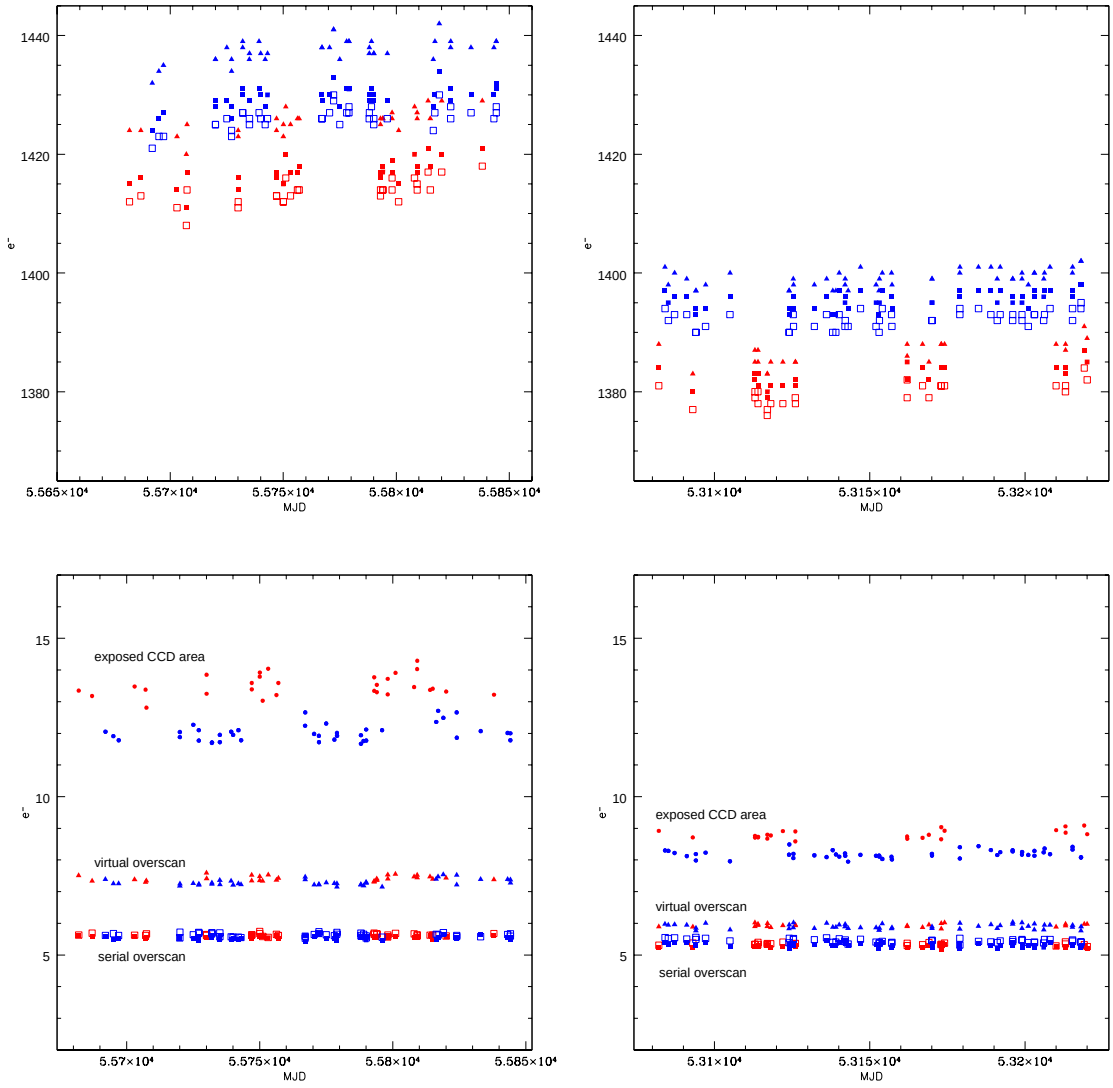

Fig. 7.— *Top panels: the average zero level as measured in the three overscan regions of the dark frames during cycle 18 (left) and 12 (right). Triangles represent the virtual overscan, solid squares the left serial overscan and empty squares the right serial overscan. Red and blue color distinguish dark frames taken at OCCDHTAV=20.977 C and 19.447 C, respectively. Bottom panels: the standard deviation (with respect to the mean value) measured in the overscan region and the exposed CCD area in dark frames taken during cycle 18 (left) and 12 (right). Solid circles represent the standard deviation of the exposed CCD area; triangles represent the standard deviation of the pixel in the virtual overscan area; solid squares represent the standard deviation of the pixels in the left serial overscan; while empty squares represent the right serial overscan. Color code is the same as in the top 2 panels.*

were taken when the detector damage due to permanence into space was certainly much smaller than at present time. Therefore we explain the difference in the zero level of the two serial overscans with an effect due to the readout electronic and exclude, instead, major CTI problems in the serial register (serial CTI). The larger value of the bias level as measured on the bottom-virtual overscan is possibly explained by the (parallel) CTI: as mentioned above the virtual overscan presents several trails due to released charges. The differences in the zero level in the three overscan regions has increased with respect to cycle 12. In addition, we have verified that the zero level of the overscan regions of dark frames is, on average, larger than the zero level of the overscan of bias frames. As, in the STIS CCD, the two serial overscans do not correspond to physical pixels (with the exception of the first raw), thermal noise cannot explain their higher zero level in dark frames with respect to bias frames and there is no obvious explanation for such a discrepancy.

The STDDEV of the three overscan regions is a proxy of the detector RON. However, when we compare the STDDEV of the overscan regions we note (see Fig. 7) that only the serial overscan (both left and right) have STDDEV which match the detector RON (as measured within the bias monitoring plan[4]); while that of the virtual overscan is higher by $\sim 2\, e^-$. Though charge traps tend to reduce the Poisson noise (and therefore the STDDEV) of a given region by removing electrons from the statistic, deferred charges from random events such as, e.g. cosmic-rays, can still impact the pixels down-stream, increasing their noise. Hence, the larger STDDEV of the virtual overscan could still be consistent with CTI effects. The fact that the RON as measured from the serial overscan region has not changed between cycle 12 and 18, implies that the amplifier noise (amplifier D in particular) has not increased with time.

When comparing the signal in the left-serial overscan region and exposed area of the detector in dark frames (Fig. 8), we notice that they have comparable scatter, while they should not. The noise contribution to the overscan region should just match the RON, while the noise contribution to the exposed area of the CCD includes also the thermal noise and noise induced by (parallel) CTI. The overscan is a measure of the image bias level and variations of the bias level from image to image as those observed in Fig. 8 might point to problems in the readout electronics (e.g. Howell 2006). This can be better seen if we consider that the scatter of the ideal overscans, whose STDDEV match the (STIS CCD) RON, should be $\simeq \frac{\sigma}{\sqrt{N}} \simeq \frac{RON}{\sqrt{N}}$ (where N is the number of frames considered), i.e. in the range 0.45-0.60 e^- for our specific case of Fig. 8, and not $\geq 1.47\, e^-$ as we observe. Note that this result does not change when the right serial overscan and/or the virtual overscan are considered. Table 1

[4]See: http://www.stsci.edu/hst/stis/calibration/Monitors/Read-Noise

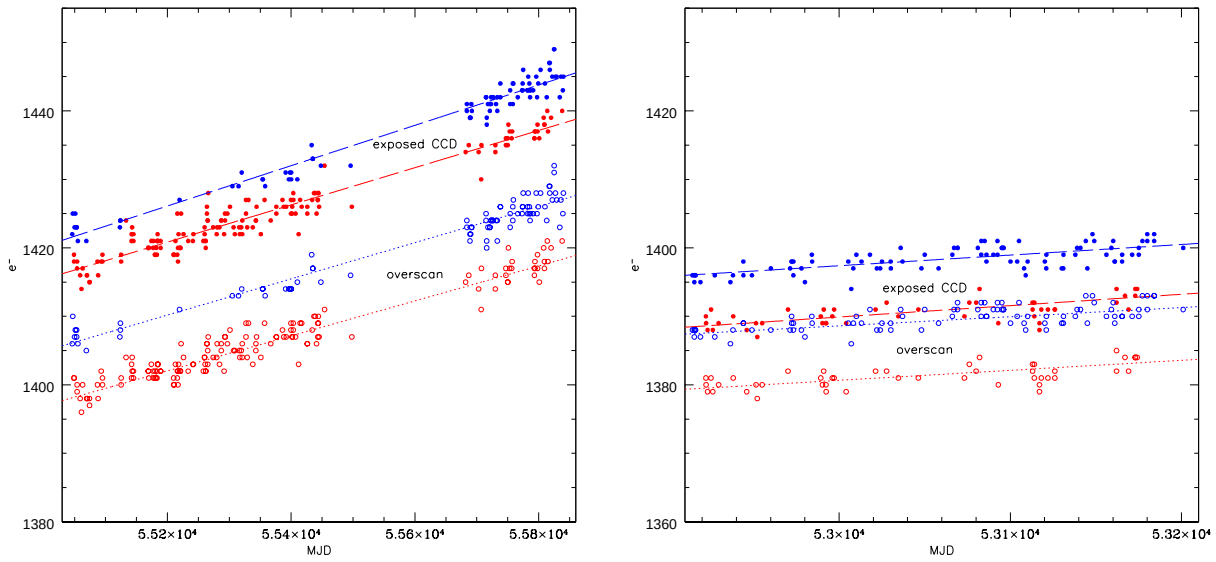

Fig. 8.— *Left panel (a): The average count level measured during cycles 17 (programs 11844 and 11845) and 18 (program 12401). Solid circles represent the average count level computed on the exposed area of the CCD. Empty circles represent the average count level in the left serial overscan area. The blue color is for the frame at OCCDHTAV temperature of 19.447 C and red color is for the frames taken at OCCDHTAV=20.977 C. Right panel (b): same as in the left panel but for the dark frames taken within programs 10018 and 10019 during cycle 12.*

reports the variance of the serial (left and right) and virtual overscan regions as measured at different epochs (aka cycles) and for different CCD-housing temperatures. The various overscan regions have comparable variances (within their uncertainties). The variances do not show any trend with the temperature, but they have increased from cycle 12 to 18.

In summary, while the "anomalies" observed in the overscan region can be explained with detector features (e.g. the roll-off) or the CTI, the actual variation of their zero level from frame to frame, seems to point to possible problems of the readout electronic. This, however, should be removed within the CALSTIS BLEV correction[5] and should not contribute to the observed dark current fluctuations. Other noise sources at the electronic level (e.g. affecting

[5]This step of the pipeline data reduction computes the zero/bias level from the overscan region of each individual (science) frame. See the STIS data handbook for more details.

			dark variance		
cycle	T (C)	N	left-SERIAL overscan	right-SERIAL overscan	VIRTUAL overscan
12b	18.0357	19	0.98 ±0.33	0.99 ±0.33	0.91 ±0.30
12b	18.3886	16	0.97 ±0.36	0.69 ±0.25	0.98 ±0.36
12b	18.7414	49	1.61 ±0.33	1.60 ±0.33	1.58 ±0.32
12b	19.0943	21	0.89 ±0.28	0.70 ±0.22	0.91 ±0.29
12b	19.4471	50	1.78±0.36	1.81 ±0.37	2.00 ±0.40
12b	19.8	32	2.10 ±0.53	2.28 ±0.58	2.20 ±0.56
12b	20.1923	23	1.97 ±0.59	2.28 ±0.67	2.45 ±0.74
12b	20.5846	17	1.45 ±0.51	1.30 ±0.46	1.59 ±0.56
12b	20.9769	24	2.06 ±0.61	2.06 ±0.61	2.39 ±0.71
17b	16.6243	17	1.45±0.51	0.78±0.28	1.60±0.57
17b	19.4471	17	1.47±0.52	1.61±0.57	1.65±0.58
17b	19.8	49	1.50±0.31	1.82±0.37	1.50±0.31
17b	20.1923	48	1.98±0.41	1.87±0.39	1.85±0.38
17b	20.5846	29	1.02±0.27	0.85±0.23	0.95±0.25
17b	20.9769	67	2.84±0.50	2.89±0.50	2.67±0.47
17b	21.3692	40	1.59±0.36	1.73±0.39	1.63±0.37
17b	21.7615	47	2.16 ±0.45	1.82±0.38	2.04±0.42
17b	22.1538	22	1.26±0.39	1.05±0.32	1.00±0.31
17b	22.5462	24	1.95 ±0.57	1.78±0.52	1.74±0.51
18b	18.7414	40	2.65 ±0.60	2.38 ±0.54	2.58 ±0.58
18b	19.0943	35	1.60 ±0.39	1.78 ±0.43	1.69 ±0.41
18b	19.4471	59	2.85 ±0.53	2.75 ±0.51	2.89±0.54
18b	19.8	43	2.28 ±0.50	1.93 ±0.42	2.11 ±0.46
18b	20.1923	28	2.18 ±0.59	2.36 ±0.64	2.08 ±0.57
18b	20.5846	17	1.67 ±0.59	1.61 ±0.57	1.80 ±0.63
18b	20.9769	29	2.91 ±0.78	2.39 ±0.64	2.11 ±0.56

Table 1: The variance (with respect to the best linear fit, which removes the time trend) of the average values in the overscan regions (serial and virtual), for group of frames at different temperatures and at different epochs. The variance and its uncertainty was estimated whenever there were at least 15 frames at a given temperature within the semester(s).

each single pixels) should be excluded because of the constant detector RON we observed over time. Hence, we conclude that the observed noise in the dark current of the exposed area of the CCD dark frames is not related to the readout electronic, nor to subsequent data processing, but most likely to CTI effect in the detector itself.

7. The pipeline temperature scaling relation and reference dark

The STScI delivers weekly reference darks which are created superposing the map of the hot pixels of the week to a so called "base-dark". The latter is created by combining a minimum of 20 (or the whole set of) dark frames taken within a given annealing period. Before being combined into a base-dark the frames are corrected for overscan and 2D normalized

bias, and scaled to a common reference temperature (currently T=18.0 C). We have used the darks from program 12401 (cycle 18) to verify the validity of the temperature scaling relation currently in use within CALSTIS. However, as the CCD-housing temperature records are on average higher than in 2001, we adopted frames at T=19.4471 C as the reference case[6]. We then followed Brown's prescription (Brown 2001a) to determine the linear temperature-scaling relation valid for normalized dark rates (see Brown 2001a for more details), deriving a steeper slope (0.09±0.02 in place of the current 0.07). The slope of the temperature scaling relation is not supposed to change with the adopted reference/denominator dark, as dividing by a dark of different temperature is equivalent to adopting a different scaling factor and just shifts the data points lower or higher in the "temperature-ratio" plane. Though the new slope possibly points to a new relation, we cannot neglect that its uncertainty is fairly large and that the two slopes are consistent within the uncertainties. The large uncertainty is an effect of the data point scatter and the fact that frames taken at a same temperature display a range of dark current values. We have verified that base-darks created using the same set of dark frames in input and the two temperature scaling relations have matching distribution and correct equally well (/poorly) a given science exposure. We conclude that there is no need, at this stage, to revise the current pipeline calibration.

8. Summary and conclusion

The STIS CCD dark current has significantly increased since cycle 12. The increased number of warm pixels explains the larger dark current. However, its larger scatter seems related to the fact that the majority of the pixels deviate from the ideal theoretical behavior expected for pixels where just the RON and dark-current Poisson-noise contribute to their noise. This noise might results from the detector CTI. A problem at the level of the readout electronic, though possibly present, can not be the major contribution to observed dark fluctuations, since it is removed during the CALSTIS processing.

The increased pixel noise has the consequence of degrading the stability of the average dark current, which means that the dark correction is no longer optimal: a number of pixels will be over-corrected (and therefore appear as negative in the 2D dark subtracted frame) while others will be under-corrected (appearing as bright pixels). However, we have verified that each of the CALSTIS steps in the data pre-processing remains useful in what each reduces the STDDEV of the pixel values in the whole frame. Note however, that the 2D bias

[6]We did not have at least one frame per annealing period at T=18.0 C, hence the choice of a different reference temperature.

subtraction reduces the *local* STDDEV only ∼50% of the time. This can be explained with the fact that the noise of the dark exposures is large enough to not be significantly improved by the bias correction, at the local level. We can recall that the bias exposures of the STIS CCD are affected by the so called "herringbone" pattern, a frequency dependent noise introduced at the readout with the side-2 electronic (see Brown 2001b, Jansen et al. 2010). Though the herringbone pattern remains visible in the bias reference frame (a normalized 2D bias image obtained by averaging ≥56 bias exposures) it affects only short exposure CCD images and certainly not the long integration time dark frames whose pixel noise is significantly larger. Therefore, the herringbone noise pattern should be a concern only in the case of short CCD exposures for which we recommend to remove it through the filtering technique described in Janesen et al. (2009). In particular we recommend to filter both bias and science frames.

The analysis and tests run insofar suggest that the most likely source of noise we observe in the dark frames is the detector CTI. The team is in the process of verifying this by modeling CTI effect similarly to ACS CCD (e.g. Anderson & Bedin 2010).

Acknowledgments

EM thanks Michael Wolfe, John Debes and especially Charles Proffit for reading the various drafts of this ISR and providing feedback, comments and valuable suggestions. EM also acknowledges the help of Tom Wheeler and Jay Anderson in clarifying (STIS) CCD architecture and behavior. Finally I thank Bryan Hilbert for running the bright-earth pointing IDL code on all cycle 17 STIS dark frames and providing me with the material to search for possible correlation between the HST pointing direction and the dark rate.

References

Anderson, J., Bedin, L., 2010, PASP, 122, 1035

Brown, T., 2001a, Instrument Science Report STIS 2001-03

Brown, T., 2001b, Instrument Science Report STIS 2001-005

Diaz, R., Technical Instrument Report 2004-01

Goudfrooij, P., Walsh. J.R., 1997, Instrument Science Report STIS 1997-09

Goudfrooij, P. et al., 2009, Instrument Science Report STIS 2009-02

Howell, S. B., 2006, "Handbook of CCD astronomy", Cambridge University Press

Jansen, R.A., Windhorst, R., Kim, H., Hathi, N., Goudfrooij, P., Collins, N., 2009, "2010 Space Telescope Science Institute Calibration Workshop", p.50

Sirianni, M., Mutchler , M., Clampin, M., Ford, H., et al., 2004, SPIE, vol.5499